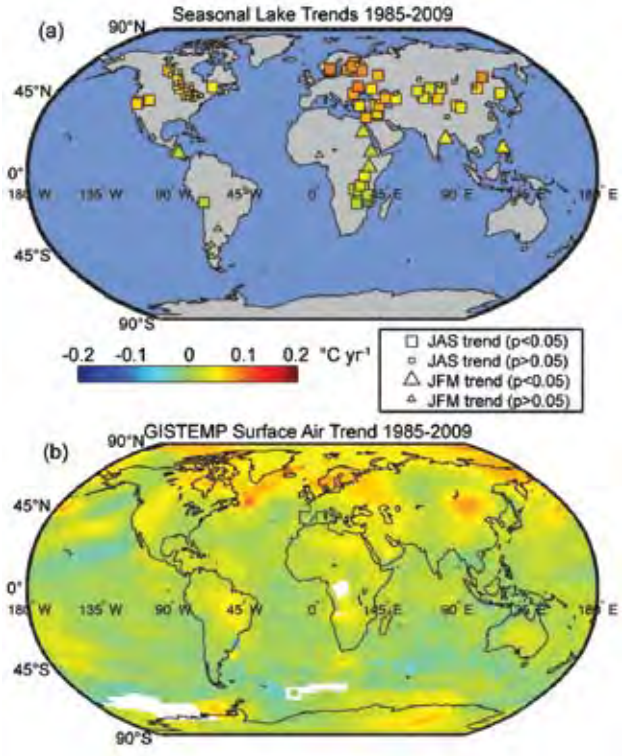

Fig. 2.10. Global (a) satellite-derived seasonal [Jul–Sep (JAS) and Jan–Mar (JFM)] nighttime lake surface temperature trends between 1985 and 2009, and (b) corresponding 1985 through 2009 JAS trends in surface air temperature obtained from GISTEMP (Hansen et al. 2006). JFM trends are not shown due to low number of JFM stations.

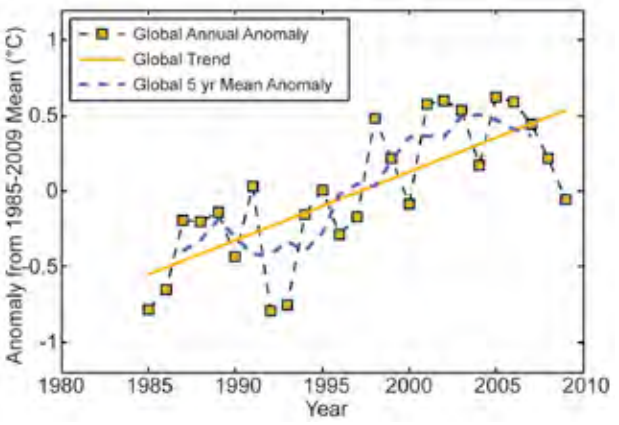

Fig. 2.11. Global average nighttime lake surface temperature anomalies averaged over all study sites.

surface air temperature analysis (Hansen et al. 2006; Fig. 2.10b) shows qualitative agreement.

The average of all time series (Fig. 2.11) highlights features such as the cooling effect caused by the 1992 Mount Pinatubo eruption and the warm anomaly caused by the strong 1998 El Niño event. The mean trend over all sites is 0.045 ± 0.011°C yr^{-1} ($p < 0.001$) and is dominated by the large number of water bodies in the midlatitudes of the Northern Hemisphere. When Northern and Southern Hemisphere are weighted equally, the global trend is 0.037 ± 0.011°C yr^{-1}. The spaceborne TIR lake temperatures provide additional independent evidence on temperature change over land and for assessing the impacts of climate change throughout the world.

c. Hydrological cycle

1) Surface humidity—K. Willett, A. Dai, and D. Berry

Surface humidity has been monitored at some sites since the 19th century (e.g., Butler and García-Suárez 2011). Only during recent decades has the coverage become near-global, by weather stations over the land and ship and buoy observations over the oceans. Historically, both specific humidity (q) and relative humidity (RH) have been derived from paired wet bulb and dry bulb thermometers. However, it is becoming increasingly common to use capacitance sensors to directly derive RH or dewpoint temperature.

There are three recent global-scale analyses of surface humidity: Dai (q and RH over land and ocean; Dai 2006); HadCRUH (q and RH over land and ocean; Willett et al. 2008); and the NOCS 2.0 (q only) ocean dataset (Berry 2009; Berry and Kent 2009). Only the NOCS 2.0 is updated to include 2010, but plans are underway to update HadCRUH over land on an annual basis, and to homogenize and update the Dai analysis. While all datasets use ship data over the ocean, HadCRUH and Dai include data from buoys, which are excluded from NOCS 2.0 owing to quality issues. All NOCS 2.0 data are then filtered by confidence in data quality and thus spatial coverage is far less than that of Dai and HadCRUH, especially over the Southern Hemisphere. NOCS 2.0 has also been bias adjusted for changes in ship height and instrument type over time and includes uncertainty estimates. Over land, Dai and HadCRUH contain many of the same station input data but methodologies are different. HadCRUH has been adjusted to remove gross inhomogeneities over land.

Recently, the ECMWF reanalysis product ERA-Interim and its predecessor ERA-40 were compared with land surface humidity from HadCRUH (Simmons et al. 2010) where good overall agreement was found. For this reason, ERA-Interim is considered suitable to monitor land surface humidity and so is used here to provide data for 2010. Other fourth generation reanalyses products are also shown where humidity fields are available for comparison.

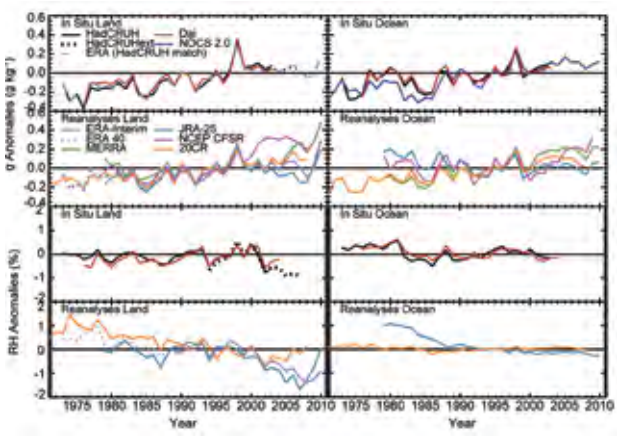

Fig. 2.12. Global average surface humidity annual anomalies. For the in situ datasets 2 m surface humidity is used over land and ~10 m over the oceans. For the reanalysis datasets, 2 m humidity is used over the whole globe. The specific humidity *(q)* and relative humidity (RH) are shown for land and ocean separately. HadCRUH, HadCRUHext, and ERA (HadCRUH match) use the 1974–2003 base period. Dai uses the 1976–2003 base period. NOCS 2.0 uses the 1971–2010 base period. The combined ERA-40 (1973–88) and ERA-Interim (1989–2010) use the 1989–2009 base period. All other reanalysis datasets use the 1989–2008 base period. All datasets are adjusted to have a mean of zero over the common period 1989–2001 to allow direct comparison. Differences in data ingestion and sea ice cover between reanalysis datasets, and in spatial coverage between reanalysis and in situ data, should be taken into account. For example, slight differences are shown between ERA spatially matched to the sampling of HadCRUH (see 'In situ Land' panel) compared to the full spatial coverage time series (see 'Reanalyses Land' panel).

Global surface moisture content, as shown by *q*, has been gradually increasing since the early 1970s, consistent with increasing global temperatures (Fig. 2.12). Trends are similar for both the land and oceans but with apparent peaks during strong El Niño events (1982/83, 1997/98). Since 1998 *q* over land has flattened somewhat but 2010 shows an increase from 2009. Although there is some spread across the datasets, there is good general agreement—less so for the reanalysis-generated ocean *q*.

Globally, specific humidity for 2010 (Plate 2.1f) strongly resembles a La Niña pattern, and is broadly consistent with that of precipitation (Plate 2.1g) and total column water vapor (Plate 2.1e). There are dry anomalies over the eastern tropical Pacific and moist anomalies over the western tropical Pacific.

ERA-Interim and HadCRUH-ext show a slight decline in global land RH from 1998 to present (Simmons et al. 2010), also shown in MERRA, consistent with a steady *q* and coincident rising temperature over this period. However, 2010 appears to be a more humid year on average. Prior to 1982, Dai and HadCRUH show positive RH anomalies over oceans. While Willett et al. (2008) speculate non-climatic causes, more recent investigation by Berry (2009) appears to implicate the North Atlantic Oscillation (NAO). RH in the reanalyses oceans is inconclusive.

2) Total column water vapor—C. Mears, J. Wang, S. Ho, L. Zhang, and X. Zhou

The map of total column water vapor (TCWV) anomalies for 2010 (Plate 2.1e) includes data both from the Advanced Microwave Scanning Radiometer EOS (AMSR-E; over the oceans; Wentz 1997; Wentz et al. 2007) and from a subset of the ground-based GPS stations with continuous data from 1997 through 2010 (J. Wang et al. 2007). This subset was chosen so that a meaningful anomaly estimate could be calculated—many more stations would be available if this

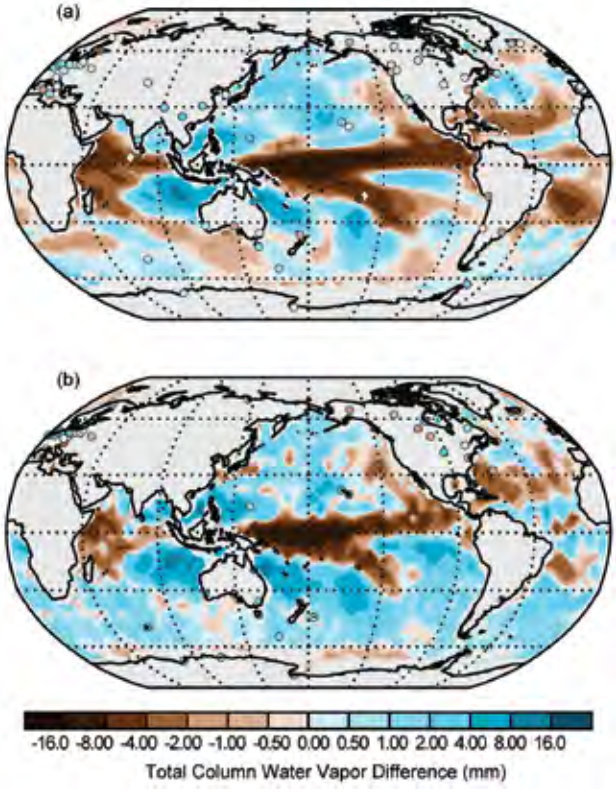

Fig. 2.13. Change in total column water vapor anomalies from Jan–Jun 2010 to Jul–Dec 2010. (a) Measurements from AMSR-E and ground-based GPS stations. (b) Measurements from COSMIC, calculated using climatological data from SSM/I and AMSR-E over ocean and using climatological data from ground-based GPS over land.